Solvent Structure and the Extended Range Hydration of Cr^{3+} in Aqueous Solution

Daniel T. Bowron*,† and Sofia Díaz-Moreno‡

ISIS Facility, Rutherford Appleton Laboratory, Chilton, Didcot OX11 0QX, United Kingdom, and Diamond Light Source Ltd., Diamond House, Harwell Science and Innovation Campus, Didcot, Oxfordshire OX11 0DE, United Kingdom

Received: May 11, 2009; Revised Manuscript Received: July 19, 2009

H/D isotopic substitution neutron scattering has been used to investigate the short and intermediate range solution structure in a 1 *m* aqueous solution of chromium nitrate. To improve the reliability of the local structural information on the cation environment, information has been incorporated from available extended X-ray absorption fine structure (EXAFS) spectroscopy data into the applied analytical framework. The markedly different structural sensitivities of the experimental probes allow the construction of a detailed three-dimensional atomistic model using the empirical potential structure refinement (EPSR) technique. The method facilitates the construction of a model that is consistent with regards to both the structural details of the immediate Cr^{3+} aqua-ion environment and the bulk hydrogen-bonded network of solvent water molecules. The results confirm the suitability of the $[Cr(H_2O)_6]^{3+}$ hydrated ion concept to describe the first hydration shell of this cation and clarify how this pseudomolecular unit is structurally incorporated in the longer range aqueous environment.

Introduction

Hydrated ion structure is often a critical factor in the chemical reactions in which an element is involved and can markedly affect the reactivity of an ion species. Chromium ion hydration is a particularly important issue due to the wide utility of the element in the modern world and where for example it is an almost unavoidable fact that the element will be present in the effluent wastes produced by the electroplating and tanning industries. This issue is currently stimulating considerable research in areas such as biosorption of chromium species[1,2] as an environmental remediation strategy. From a more fundamental viewpoint, the hydration of chromium ions has also played an important role in the development of the theory of electron transfer reactions where the structural stability of the $[Cr(H_2O)_6]^{3+}$ aqua ion allowed Taube to investigate the mechanism of the transfer of electrons of nonmetal oxidants with a hydrated ion species.[3]

Key findings of Hunt and Taube's[4] work on the Cr^{3+} aqua ion were the 6-fold stoichiometry of the hydrated ion and the surprising stability of this structure against exchange of water molecules from the immediate hydration shell to the bulk. The half-life for the exchange mechanism was found to be ~40 h at 25 °C.[4] Experimentally, the structure of this hydrated ion has been tested extensively by neutron scattering,[5] X-ray diffraction,[6,7] and EXAFS spectroscopy,[8,9] where the interest in the structure of the ion moved outward from the immediate structure of the first hydration shell of six water molecules, to the more distant intermolecular correlations by which the hydrated ion complex is incorporated into the larger solvent water network. However, as the sensitivity of the experimental probes was unavoidably dominated by the immediate ion hydration environment, most progress in establishing the details of the longer range structure has largely been restricted to computational investigations.[10,11]

In this work, we report a different approach to the structural characterization of the Cr^{3+} aqueous solutions, in which we complement the analysis of neutron scattering with H/D isotopic substitution experimental data with available EXAFS spectroscopy data to refine a three-dimensional atomistic model of the system that is consistent with experimentally constrained chemically specific local and bulk solution structure. The spectroscopic information provides detailed insight into the immediate Cr^{3+} hydration environment, while through the appropriate choice of isotopic substitution measurements, the neutron scattering data are weighted toward the structural correlations between the solvent water molecules. As the short-range (ion) and bulk (solvent) structural correlations are thus strongly constrained, this analytical strategy allows us to increase our confidence in any structural conclusions we draw on the interatomic and intermolecular correlations that occur in and beyond the ion's second hydration shell.

Experiment

To facilitate the construction of a comprehensive structural model of chromium nitrate solutions, hydrogen−deuterium isotopic substitution neutron scattering methods have been used. By performing neutron scattering measurements on three 1 *m* solutions of $Cr(NO_3)_3$ prepared in H_2O, in D_2O, and in a 1:1 mixture of H_2O and D_2O, it is possible to strongly weight the structural information accessible from the data toward the correlations that occur between the water molecules.[12] Approximately 3 cm^3 of each isotopic solution was prepared by weight to ensure equivalence of the solution stoichiometry. Each sample was prepared by dissolving the appropriate amount of $Cr(NO_3)_3 \cdot 9H_2O$ (Sigma-Aldrich 99.99%) in H_2O, D_2O (Sigma-Aldrich 99.9 atom % D), and the 1:1 H_2O:D_2O mixture to give samples with a Cr^{3+} ion to water molecule ratio of 1:55.5. For the D_2O containing samples, allowance was made during the data reduction and modeling procedures for the small quantity of H_2O that was carried into the solutions by the nonahydrated salt. To prevent hydrolysis of the samples, each solution was acidified to a pH of ~1 by the addition of a small quantity

* Corresponding author. E-mail: daniel.bowron@stfc.ac.uk.
† ISIS Facility.
‡ Diamond Light Source Ltd.

10.1021/jp904382n CCC: $40.75
Published on Web 08/12/2009

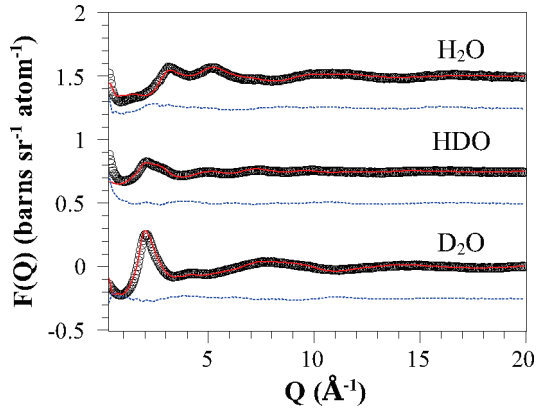

Figure 1. The EPSR model fits (red solid line) and fit residuals (blue dotted line) to the isotopic samples of 1 *m* $Cr(NO_3)_3$ solutions prepared from D_2O, HDO, and H_2O. The experimental data are shown as "○". For clarity, the model fits and experimental data are vertically offset by 0.0, 0.75, and 1.5 units, respectively, for the D_2O, HDO, and H_2O solutions, while the corresponding fit residuals are vertically offset by −0.25, 0.5, and 1.25 units.

(∼0.01 g) of concentrated (65%) HNO_3. For the neutron scattering measurements, 1.4 cm^3 of each of the solutions was transferred to $Ti_{0.676}Zr_{0.324}$ alloy cells, where the cell walls of 1 mm thickness define an internal sample volume of dimensions 1 mm thickness × 35 mm width × 40 mm height. By virtue of the combination of the Ti and Zr neutron scattering lengths ($b_{Ti} = -0.344$ and $b_{Zr} = +0.716$) and the alloy composition, the cell makes no contribution to the coherent scattering signal from the sample. The filled cells were loaded onto the automatic sample changer of the small-angle neutron diffractometer for amorphous and liquid samples (SANDALS) at the ISIS pulsed neutron source of the Rutherford Appleton Laboratory, UK. This instrument is specifically optimized, through the use of high energy neutrons and scattering angles below 40°, to perform neutron scattering measurements on samples containing light elements while minimizing the parasitic effects of inelastic scattering on the structural data that are caused by the similarity in mass of the scattered neutron and the scattering atoms. The temperature of each sample was controlled to be 25 ± 0.1 °C. The experimental data were corrected for background scattering, absorption, multiple scattering, and normalized to the scattering from a vanadium standard using the Gudrun routines that are based on the algorithms of the widely used ATLAS package.[13] The resulting functions were corrected for the self and inelastic scattering contributions following the methods of Soper and Luzar[14] that resulted in the interference differential scattering cross sections $F(Q)$ shown in Figure 1. $F(Q)$ is defined as

$$F(Q) = \sum_{\alpha \le \beta} (2 - \delta_{\alpha\beta}) c_\alpha c_\beta b_\alpha b_\beta [S_{\alpha\beta}(Q) - 1] \qquad (1)$$

Q is the magnitude of the momentum transfer vector of the scattering process, defined as $Q = 4\pi \sin\theta/\lambda$, where λ is the wavelength of the incident neutron and θ is one-half the scattering angle, c_α and c_β are the concentrations of the atomic species α and β, while b_α and b_β are their neutron scattering lengths.[15] $S_{\alpha\beta}(Q)$ are the partial structure factors representing pairwise structural correlations between the atoms, and $\delta_{\alpha\beta}$ is the Kronecker delta function to avoid double counting the correlations between like atomic species. $S_{\alpha\beta}(Q)$ is related to the corresponding real space partial pair distribution functions, $g_{\alpha\beta}(r)$, by a Fourier transform weighted by the atomic density, ρ, of the system under study.

$$[g_{\alpha\beta}(r) - 1] = \frac{1}{2\pi^2\rho}\int_0^\infty Q^2[S_{\alpha\beta}(Q) - 1]\frac{\sin Qr}{Qr}dQ \qquad (2)$$

TABLE 1: Relative Contributions of the Partial Structure Factors to the Total Interference Differential Scattering Cross Section of a 1 *m* Solution of $Cr(NO_3)_3$ in D_2O

pair correlation	percentage weight
Cr−Cr	0.001
$Cr-N_{NO_3^-}$	0.023
$Cr-O_{NO_3^-}$	0.043
$Cr-O_{water}$	0.255
$Cr-H_{water}$	0.435
$N_{NO_3^-}-N_{NO_3^-}$	0.092
$N_{NO_3^-}-O_{NO_3^-}$	0.341
$N_{NO_3^-}-O_{water}$	2.038
$N_{NO_3^-}-H_{water}$	3.471
$O_{NO_3^-}-O_{NO_3^-}$	0.318
$O_{NO_3^-}-O_{water}$	3.790
$O_{NO_3^-}-H_{water}$	6.456
$O_{water}-O_{water}$	11.31
$O_{water}-H_{water}$	38.53
$H_{water}-H_{water}$	32.82

If only a single neutron scattering measurement is made, it is not possible to separate all of the partial structure terms that contribute to the interference differential scattering cross section, and a composite structure factor and corresponding pair distribution function is obtained. Table 1 shows the relative contributions of the various partial distribution functions to the total interference differential scattering cross section for a 1 *m* $Cr(NO_3)_3$ in D_2O solution. This clearly demonstrates that the sensitivity of the neutron scattering data on this solution is almost entirely weighted toward structure of the solvent water itself, with the cation hydration only contributing ∼0.5% to the total signal in the D_2O $F(Q)$.

Data Modeling

To facilitate the extraction of the structural information from the neutron scattering $F(Q)$'s, the data have been modeled using the empirical potential structure refinement procedure developed by Soper.[16,17] This method uses the available experimental scattering data to generate a set of interatomic perturbation potentials that are used to drive a classical Monte Carlo simulation of the system into structural configurations that agree with the driving $F(Q)$'s. This analytical framework ensures that the resulting three-dimensional atomistic structural model is consistent with the basic physicochemical constraints of the system's bulk atomic density and the known conformations of the molecular units from which it is built. A particular advantage of the approach is that once an acceptable model has been built it is possible to interrogate the structure and obtain an estimate of any of the atomic partial pair distribution functions, despite the fact that only a subset are fully constrained by the experimental data. However, it is important to recognize that any pair distribution functions not heavilly constrained by the scattering data will primarily reflect the prior assumptions made for the underlying interatomic interaction potentials, the packing requirements that result from the imposed basic geometries of the molecules, and the requirement that the model conforms to the known bulk density of the system under study. However,

TABLE 2: Lennard-Jones and Charge Parameters Used in the Simulation of $Cr(NO_3)_3$ Solutions[a]

atom	ε [kJ/mol]	σ [Å]	q [e]	mass [amu]
Cr	0.1250	2.260	+3.0000	52
H_{H^+}	0.0075	1.000	+1.0000	2
$N_{NO_3^-}$	0.8374	3.900	0.8603	14
$O_{NO_3^-}$	0.6490	3.154	−0.6201	16
O_{water}	0.6500	3.160	−0.8476	16
H_{water}	0.0000	0.000	0.4238	2

[a] Within the EPSR model, these are combined using the Lorenz−Berthelot mixing rules $\sigma_{\alpha\beta} = 1/2[\sigma_\alpha + \sigma_\beta]$ and $\varepsilon_{\alpha\beta} = [\varepsilon_\alpha \varepsilon_\beta]^{(1/2)}$.

provided that these three primary constraints are reasonable, the models can provide a useful guide for improving our general understanding of how the structure of the system gives rise to its observed physical and chemical properties.

To model the 1 *m* aqueous solution of $Cr(NO_3)_3$, a model containing 20 Cr^{3+} ions, 60 NO_3^- ions, and 1110 water molecules was constructed in a cubic box of side length ~33 Å, corresponding to the measured atomic density of the solutions of 0.1 ± 0.005 atoms $Å^{-3}$. To allow for the small amount of nitric acid added to acidify the solutions to pH ≈ 1, an additional two H^+ and two NO_3^- ions were added to the model. The Lennard-Jones and charge parameters used to describe the reference potentials for the model components are given in Table 2. The parameters for the reference potential used for the water molecules in the simulation are taken from the SPC/E model of Berendsen et al.,[18] while the parameters for the nitrate ion were taken from Krienke and Opalka.[19]

These reference potentials are first used to equilibrate the Monte Carlo simulation of the solution, after which the EPSR algorithm is turned on and the experimental data are used to derive the set of perturbation functions that will then drive the structural configurations into consistency with the scattering data. Once this is achieved, the simulation is continued, and ensemble average information is accumulated on the structural configurations of the atoms and molecules. These data can include the partial distribution functions, bond angle distributions, and coordination number histograms etc.

Figure 1 shows the fits and fit residuals for the EPSR model of the 1 *m* $Cr(NO_3)_3$ aqueous solution, as compared to the experimental neutron scattering data from the three isotopic solvent variants, H_2O, D_2O, and HDO.

To assist in the modeling of the $Cr(NO_3)_3$ solutions, an additional constraint was included in the EPSR model. This constraint is based on the well-known chemistry of the Cr^{3+} aqua ion and its highly stable 6-fold coordination.[4] Instead of treating all of the water molecules in the simulation as independent entities, the Cr^{3+} ions were incorporated into the model as a hydrated molecular ion consisting of six water molecules bound to each Cr^{3+} site in an octahedral local geometry with regards to the distribution of the six water oxygen sites. This approach follows the work of Pappalardo[10] and Martínez,[11] although the mechanism for incorporating a molecular species into the EPSR simulation differs in the details from the approach used in these earlier studies due to the need for intramolecular structural disorder.

The difference in how molecular species are incorporated into EPSR models arises from the requirement of the simulations to reproduce experimental scattering data. In measured data, each intramolecular atomic distance correlation is found to have a finite width and is a consequence of each molecule in the sample, in the instantaneous structural snapshot of the scattering experiment, reflecting a slightly different conformation. This is due to the disorder introduced by the zero point energy that allows the atoms in the molecule to vibrate within their bonding potentials. To capture this issue, the intramolecular bonds within the molecules of an EPSR simulation are constrained to reflect a distribution in their lengths using a simple harmonic potential $U_{intra}(r)$.[20] This is defined as:

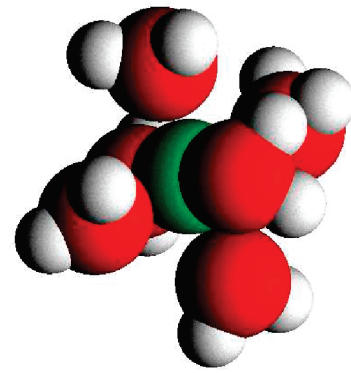

Figure 2. Snapshot of a $[Cr(H_2O)_6]^{3+}$ molecular ion taken from the EPSR simulation. This figure provides an example of the structural disorder that EPSR introduces into the molecular geometry to allow experimental scattering data to be modeled effectively.

$$U_{intra}(r) = C \sum_i \sum_{\alpha\beta \neq \alpha} \frac{(r_{\alpha\beta_i} - d_{\alpha\beta})^2}{2w_{\alpha\beta}^2} \quad (3)$$

$r_{\alpha\beta_i}$ is the actual separation of the atoms α and β in molecule i, and $d_{\alpha\beta}$ is the average distance of the bond between the atoms.

$$w_{\alpha\beta}^2 = \frac{d_{\alpha\beta}}{\sqrt{\mu_{\alpha\beta}}} \quad (4)$$

and

$$\mu_{\alpha\beta} = \frac{M_\alpha M_\beta}{(M_\alpha + M_\beta)} \quad (5)$$

is the reduced mass of the atom pair $\alpha\beta$. M_α and M_β are the mass of each atom in atomic units, and C is a constant that has been empirically determined from the scattering data, where a value of 130/Å·amu$^{1/2}$ has been found to give good reproduction of the widths of the intramolecular structural features found in experimentally determined radial distribution functions.

An advantage of using this harmonic force model to periodically disorder the structure of the molecules in the EPSR model is that this avoids the problem of a proliferation of structural parameters. The force is naturally related to the masses of the atoms involved in each bond and circumvents the need to refine individual Debye−Waller factors for every bond in every molecule type, included in the simulation. All that is required in the EPSR simulation is to define the average bond lengths, $d_{\alpha\beta}$, found in each molecule. Figure 2 shows a typical snapshot of a hydrated $[Cr(H_2O)_6]^{3+}$ molecular ion taken from the EPSR simulation to illustrate the structural disorder introduced into the molecular structure. The average structure of the molecular ion was constrained to give mean Cr−O and Cr−H distances of 1.97 and 2.66 Å, while the water molecules were constrained to give O−H and H−H distances of 0.976 and 1.55 Å. The

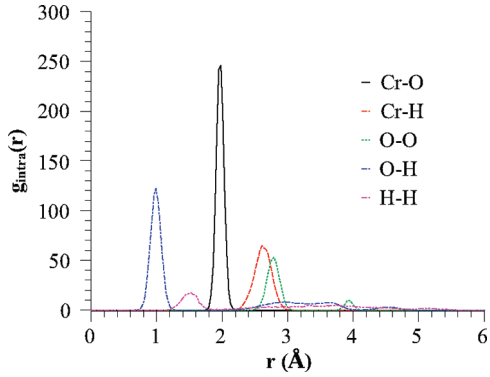

Figure 3. Intramolecular pair distribution functions calculated as an ensemble average of several hundred snapshots of the $[Cr(H_2O)_6]^{3+}$ ion generated by the EPSR simulation.

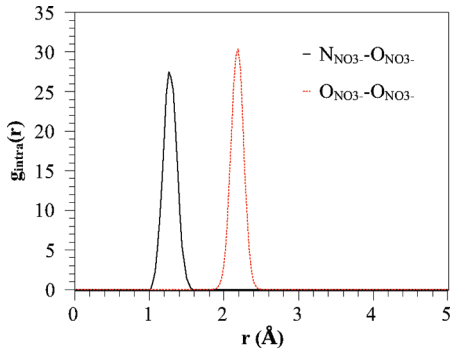

Figure 4. Intramolecular pair distribution functions calculated as an ensemble average of several hundred snapshots of the $[NO_3]^-$ ion generated by the EPSR simulation.

correlations between oxygen atoms on different water molecules were constrained to be 2.78 and 3.93 Å depending on whether the molecules were adjacent to each other or bridged across the Cr^{3+} ion. The disorder in the configuration can be seen in the range of orientations adopted by the water molecules in the Cr^{3+} hydration shell.

Figure 3 shows the intramolecular partial distribution functions for the hydrated Cr^{3+} molecular ion shown in Figure 2. These are calculated by ensemble averaging over several hundred snapshots of the structure during the course of the EPSR simulation. The widths of the peaks in these functions illustrate how the harmonic bond potential model implemented in the refinement process broadens the peaks to introduce structural disorder into the pair distribution functions.

The nitrate counterion has been incorporated into the EPSR model as an unhydrated entity as the residence time of the water molecules in its hydration shell is orders of magnitude shorter than that found for the hydrated Cr^{3+} ion, with typical values of ~1 ps.[21] The structure of the molecular anion was incorporated into the model defined with the site−site Lennard-Jones and charge parameters given in Table 2 and specifying mean $N_{NO_3^-}-O_{NO_3^-}$ and $O_{NO_3^-}-O_{NO_3^-}$ distances of 1.27 and 2.20 Å, respectively. Figure 4 shows the corresponding intramolecular pair distribution functions generated by the harmonic model of the $[NO_3]^-$ ion.

Testing the Model of the Local Cr^{3+} Hydration Structure

To test the reliability of the structure of the local Cr^{3+} ion environment captured in the EPSR model, it is necessary to calculate an experimentally accessible function that is strongly weighted to the local regions of the solution in which the ions

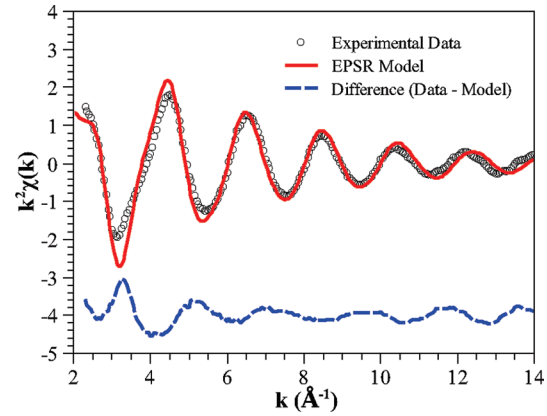

Figure 5. Cr K-edge EXAFS data (○)[8] obtained from an aqueous solution of $Cr(NO_3)_3$ and the EXAFS signal calculated from the EPSR model (red solid line) using the FEFF 8 code.[25] Values for the two free parameters in the EXAFS theory, S_0^2 and E_0, used in the EPSR-EXAFS calculation were 0.955 and 6.0 eV, respectively. S_0^2 was estimated by the FEFF 8 package, and E_0 was chosen to best phase the calculated signal with the experimental data. The difference function (blue broken line) between the experimental data and the simulated signal is shown offset vertically by −4.0 units.

are found. An extended X-ray absorption fine structure (EXAFS) spectrum is just such an appropriate signal. The experimental technique is chemically specific and can provide accurate local structural information out to a distance of ~4 Å from the target atomic site. Information is accessible on the radial distances to neighboring atoms and on their chemical type and number. Recent developments in the EPSR technique now allow us to calculate EXAFS spectra from the atomistic models, and consequently we can now test how well dilute solute species have been incorporated in the models that have been generated from the bulk structure sensitive diffraction data.[22−24] All of the EXAFS spectra calculations were performed using the FEFF 8 code,[25] and ~8000 Cr sites were investigated to generate the ensemble average signal.

For the Cr^{3+} system investigated here, this test is particularly important because it will allow us to evaluate the quality of the hydrated molecular ion concept, as implemented in the EPSR procedure. Figure 5 shows that the EXAFS signal calculated from the model is in good agreement with the spectrum available in the literature[8] despite the fact that the concentration of the solution studied here is 10 times more concentrated at 1 *m* as opposed to the published measurement at 0.1 *m*. This difference in concentrations has been assumed to be negligible because the measured spectra from the $Cr(NO_3)_3$ solutions were found to be identical in the $[Cr^{3+}]$ concentration range from 0.005 to 2.6 *m*,[8] which is probably the result of the resilience of the $[Cr(H_2O)_6]^{3+}$ pseudomolecular unit in aqueous solution.

The highly comparable quality of the EXAFS spectrum calculated from the EPSR model with the experimental EXAFS data, particularly beyond $k \approx 5$ Å^{-1}, indicates that the implementation of the hydrated ion concept within the simulation is reasonable with respect to the structural information contained in the measured EXAFS signal. The observation that the decay envelope of the calculated signal agrees with the experimental data demonstrates the suitability of the harmonic model for describing the intramolecular bond disorder. The slight misfit in the low-*k* region of the spectrum is thought to be indicative of imperfect multiple scattering captured either by the EPSR model or by approximations in the EXAFS theory itself. This spectral region is particularly sensitive to both multiple scattering of the photoelectron and the detailed form

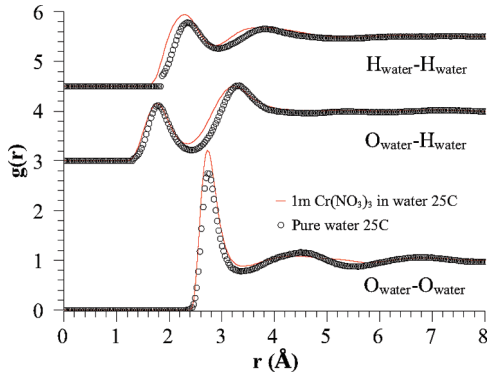

Figure 6. Solvent water partial distribution functions $O_{water}-O_{water}$, $O_{water}-H_{water}$, and $H_{water}-H_{water}$ (lines) in a 1 *m* $Cr(NO_3)_3$ solution, as compared to the corresponding functions (○) for the pure liquid.[20] The water correlations in the $Cr(NO_3)_3$ solution do not include the contributions of the six water molecules bound in the first hydration shell of each Cr^{3+} ion.

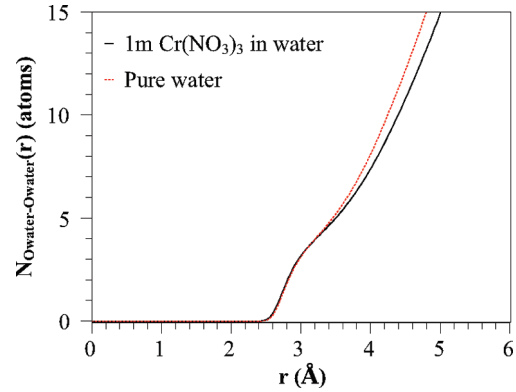

Figure 7. Running coordination number $N_{O_{water}-O_{water}}(r)$ for a 1 *m* $Cr(NO_3)_3$ solution (black solid line), as compared to the corresponding function for the pure liquid (red broken line).

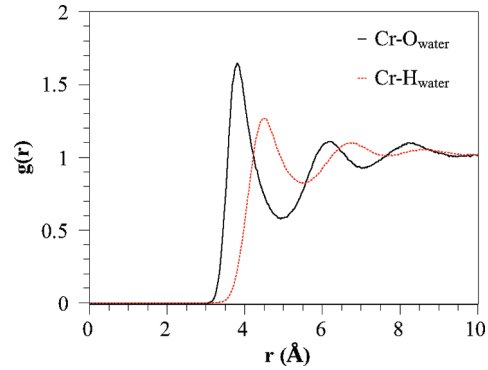

Figure 8. Pair distribution functions relating the hydration of the $[Cr(H_2O)_6]^{3+}$ hydrated ion: $g_{Cr-O_{water}}(r)$ (black solid line) and $g_{Cr-H_{water}}(r)$ (red broken line).

of the atomic scattering potentials. Any error in the approximations used in deriving the scattering potentials would make a cumulative contribution to the calculated multiple scattering signals. As the atomistic model produced by EPSR intrinsically includes the hydrogen sites in the cluster models, it is a particular challenge to specify ideal scattering potentials for the signal calculations.[26] This coupled effect is thus considered the most probable source of the slight misfitting at low-*k*. However, these issues aside, the overall quality of the predicted EXAFS signal is sufficient to give us confidence that we can safely proceed to investigate the longer range solution structure that is more strongly constrained by the diffraction data.

General Solution Structure

Solvent Structure. A brief consideration of Table 1 tells us that basing the EPSR model on the neutron scattering data will provide rigorous constraints on the bulk structure of the solution. In particular, the structural correlations between the water molecules make prominent contributions to the experimental data and correspondingly to the refined model. Figure 6 shows the solvent water partial distribution functions obtained from the EPSR model of the chromium nitrate solution, as compared to the corresponding functions for the pure solvent.[20]

The $O_{water}-O_{water}$ partial distribution function is the most informative regarding the structure of the solvent water. Although the first peak in this function for the $Cr(NO_3)_3$ solution appears larger than the corresponding feature for the pure liquid, the running coordination number (Figure 7) tells us that each water molecule remains, on average, tetrahedrally coordinated to ~4 neighboring water molecules in the first hydration shell. Real differences, however, begin to appear at the second neighbor correlation level corresponding to the distance range from ~3 to ~6 Å where $g_{O_{water}-O_{water}}(r)$ shows that the second shell in the salt solution is more poorly defined than in the pure liquid. This suggests that the presence of the ions in the solution is tending to disorder the longer range correlations in the solvent water network.

A comparison of $g_{O_{water}-H_{water}}(r)$ confirms that the intermolecular hydrogen bonding between the water molecules, in both the salt solution and pure water, is very similar. Integration of the first peak in this function tells us that each water oxygen atom is indeed hydrogen bonded to the hydrogen sites of two neighboring water molecules and that each hydrogen on a water molecule makes one hydrogen bond to a neighboring water molecule oxygen site. The presence of the $[Cr(H_2O)_6]^{3+}$ and NO_3^- ions in the solution therefore does not appear to compromise the ability of the solvent to fully establish its hydrogen-bonded network.

Last, comparing $g_{H_{water}-H_{water}}(r)$ between the salt solution and pure water suggests that the presence of the ions encourages a slightly closer packing of the hydrogen sites between neighboring water molecules, and this effect can also be seen in the second peak of the $g_{O_{water}-H_{water}}(r)$ distribution function telling us about the packing of the water hydrogen sites with respect to the water oxygen positions in the solution.

Ion Hydration. Having established that the $[Cr(H_2O)_6]^{3+}$ hydrated ion model is a good representation of the short-range structure around the chromium sites in the solution, the benefit of the bulk structural model is that it is now possible to investigate the more distant structural correlations between the ion sites, and the solvent and other ions. Figure 8 shows the $g_{Cr-O_{water}}(r)$ and $g_{Cr-H_{water}}(r)$ pair distribution functions that effectively tell us about the second and more distant hydration shells of the Cr^{3+} sites.

The existence of at least three well-defined oscillations in both the $Cr-O_{water}$ and the $Cr-H_{water}$ partial distribution functions tells us that the hydration structure of the Cr^{3+} ions appears to structure the solvent out to at least the fourth hydration shell of the bare ion. This ordering of the hydration water molecular configurations is manifest in both the oxygen and the hydrogen correlations, and $g_{Cr-H_{water}}(r)$ is consistently out of phase with $g_{Cr-O_{water}}(r)$. This signal phasing indicates that the orientational correlations between the water molecules in the succesive hydration shells are being maintained and propagated on the hydrogen-bonded network in the solvent.

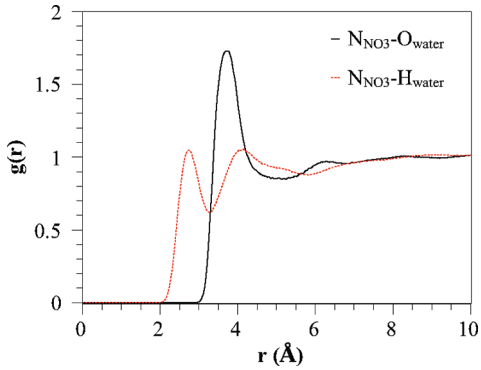

Figure 9. Pair distribution functions relating the hydration of the NO_3^- ions: $g_{N_{NO_3^-}-O_{water}}(r)$ (black solid line) and $g_{N_{NO_3^-}-H_{water}}(r)$ (red broken line).

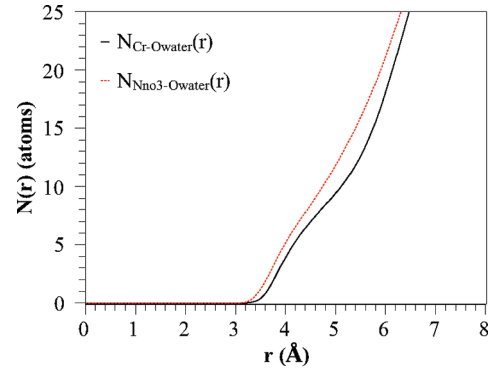

Figure 10. Running coordination number of water oxygen atoms about the center of the $[Cr(H_2O)_6]^{3+}$ (black solid line) and the NO_3^- ions (red broken line).

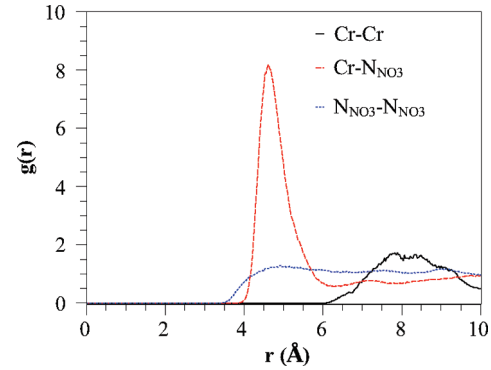

Figure 11. Pair distribution functions relating the ion−ion interactions in the 1 *m* $Cr(NO_3)_3$ solution: $g_{Cr-Cr}(r)$ (black solid line), $g_{Cr-N_{NO_3^-}}(r)$ (red dashed line), and $g_{N_{NO_3^-}-N_{NO_3^-}}(r)$ (blue dotted line).

For comparison, Figure 9 shows the corresponding pair correlation functions for the hydration of the nitrate anions, $g_{N_{NO_3^-}-O_{water}}(r)$ and $g_{N_{NO_3^-}-H_{water}}(r)$. For clarity, it is worth pointing out that as these correlations are weakly weighted in the neutron diffraction data used to refine the EPSR model, and in the absence of spectroscopic information on the local environment of the nitrogen sites to benchmark the model, these structural correlations are predominantly dependent on the quality of the reference potential parameters[19] used in the simulation of the data.

The behavior of $g_{N_{NO_3^-}-O_{water}}(r)$ and $g_{N_{NO_3^-}-H_{water}}(r)$ shows that the extended range hydration structure of the NO_3^- anions is considerably more disordered than the Cr^{3+} cations. Only the first hydration shell is strongly defined for the water oxygen site correlations, although there are two clearly defined shells of water hydrogens. As the correlations in the region that would correspond to the second oxygen shell are diffuse and poorly defined, this indicates a loss of strong orientational ordering from the ion beyond its immediate solvation shell. This result is clearly consistent with the smaller charge on this ionic species and the knowledge that the water molecules in the anion first hydration shell are more mobile than those found in the corresponding environment of the Cr^{3+} cation. The integral of the first peak of $g_{N_{NO_3^-}-H_{water}}(r)$ to a distance of 3 Å shows that there are ∼3 water hydrogen atoms bound at this distance, one for each of the oxygen atoms of the NO_3^- ion. The second peak in $g_{N_{NO_3^-}-H_{water}}(r)$ integrated between 3 and 4.5 Å is found to include a further ∼13 water hydrogens.

Considering the ion−O_{water} correlations shown in Figures 8 and 9, it is an interesting observation that the second hydration shell of the Cr^{3+} ion is comparable in size to the first hydration shell of the NO_3^- ion. The number of water molecules involved in this shell can be seen in the running coordination number of water oxygens about each of the ions (Figure 10). At a radial distance of 5.1 Å, the Cr^{3+} ion has ∼10 water molecules in its second hydration shell, while the NO_3^- has ∼12 water molecules in its first hydration shell.

Ion−Ion Correlations. The final aspect of the solution structure are the ion−ion correlations. At the investigated solution concentration of 1 *m*, it is experimentally impossible to get direct information on this aspect of the system. In the diffraction data, the ion−ion correlation functions contribute <1% to the total signal, while in the EXAFS signal the ion−ion correlations tend to be very weak due to the high degree of structural disorder and their relatively distant correlation length. In the case of nitrate solutions, the EXAFS probe also faces an additional issue of ambiguity given the similarity in atomic number between the water oxygen atoms and the oxygen and nitrogen atoms of the anion.

As the EPSR refinement is based upon an atomistic model, it is in this case possible to obtain estimates of the likely ion−ion interactions that take place in the solution, subject to the constraints imposed by the charges defined in the reference potentials and the need for the bulk structural correlations to reproduce the diffraction data. Figure 11 shows the correlations between the chromium and nitrogen sites that reflect the ion−ion interactions in the model.

Because of the strongly hydrated nature of the Cr^{3+} cation and the relatively high electrical charge, the average Cr−Cr correlation appears to be centered around 8 Å. Both the Cr−$N_{NO_3^-}$ and the $N_{NO_3^-}$−$N_{NO_3^-}$ close correlations begin at ∼4 Å, with the $g_{Cr-N_{NO_3^-}}(r)$ indicating a strong preference for ion-paired correlations centered at 4.6 Å, effectively bridged by the water molecules in the first hydration shell of the cation. The integral of this peak tells us that each Cr^{3+} ion has ∼3.5 NO_3^- ions in the region out to 6 Å radius from the cation, and these effectively act as a screen for more distant solution molecules against the large charge associated with the chromium sites. The $N_{NO_3^-}$−$N_{NO_3^-}$ correlations, although starting at a similar distance to the Cr^{3+}−$N_{NO_3^-}$ correlations, are highly diffuse and show that there is little preference for pairing between themselves.

Conclusions

In conclusion, this study has shown that EPSR applied to neutron scattering data has allowed the construction of a comprehensive model of the structure of a 1 *m* $Cr(NO_3)_3$ solution. The bulk structural correlations between the solvent water molecules were strongly constrained by the scattering data,

while EXAFS signals calculated for the local environment around Cr^{3+} ion sites enabled us to confirm the suitability of the hydrated ion model to describe the local structural environment of the cations in solution. The combination of this bulk and local structure sensitivity thus provided a firm foundation from which the longer range structural correlations in the solution could be explored.

The effect of the Cr^{3+} and NO_3^- ions on the solvent water itself was primarily found to be manifest as increased disorder in the second neighbor correlations between water molecules. The first neighbor interactions remain largely tetrahedral and highly comparable to those found in the pure liquid, and the hydrogen-bonding network between the molecules appears to remain intact. The increased disorder in the more distant water molecule correlations appears to arise from a slightly more dense packing of the hydrogen sites on the molecules.

Accepting that the first hydration shell of the Cr^{3+} ion consists of six firmly bound water molecules, the bulk structural model showed that, as a result, the cation hydration is strongly templated in shells of water oxygen and hydrogen correlations out to four layers from the bare ion. This contrasts with the findings for the NO_3^- anion where only its first hydration shell is well-defined. An interesting observation was the approximate equivalence in the size of the single shell hydrated anion with the double shell hydrated cation.

Last, it was possible to use the three-dimensional model to estimate the extent of the ion−ion correlations in this relatively dilute solution. Each chromium ion was found to have ∼3.5 nitrate anions bound to its first hydration shell. This effectively allows charge neutrality to be maintained throughout the bulk of the solution, but also tells us that the ability of the Cr^{3+} to strongly orient the water molecules over several hydration shells is sufficiently dominant not to be significantly perturbed by the presence of three to four nitrate anions in its local vicinity.

Acknowledgment. We thank the ISIS Pulsed Neutron and Muon Facility for access to neutron beamtime and support facilities.

References and Notes

(1) Chergui, A.; Bakhti, M. Z.; Chahboub, A.; Haddoum, S.; Selatnia, A.; Junter, G. A. *Desalination* **2007**, *206*, 179–184.
(2) Sahmoune, M. N.; Louhab, K.; Boukhiar, A. *Environ. Res. J.* **2008**, *2*, 254–260.
(3) Taube, H. *Nobel Lectures, Chemistry 1981−1990*; World Scientific Publishing Co.: Singapore, 1992.
(4) Hunt, J. P.; Taube, H. *J. Chem. Phys.* **1950**, *18*, 757–758.
(5) Broadbent, R. D.; Neilson, G. W.; Sandström, M. *J. Phys.: Condens. Matter* **1992**, *4*, 639–648.
(6) Caminiti, R.; Licheri, G.; Piccaluga, G.; Pinna, G. *J. Chem. Phys.* **1978**, *69*, 1–4.
(7) Lindqvist-Reis, P.; Munoz-Páez, A.; Díaz-Moreno, S.; Pattanaik, S.; Persson, I.; Sandström, M. *Inorg. Chem.* **1998**, *37*, 6675–6683.
(8) Munoz-Páez, A.; Pappalardo, R. R.; Sánchez-Marcos, E. *J. Am. Chem. Soc.* **1995**, *117*, 11710–11720.
(9) Sakane, H.; Munoz-Páez, A.; Díaz-Moreno, S.; Martínez, K.; Pappalardo, R.; Sánchez-Marcos, E. *J. Am. Chem. Soc.* **1998**, *120*, 10397–10401.
(10) Pappalardo, R. R.; Martínez, J. M.; Sánchez-Marcos, E. *J. Phys. Chem.* **1996**, *100*, 11748–11754.
(11) Martínez, J. M.; Pappalardo, R. R.; Sánchez-Marcos, E.; Refson, K.; Díaz-Moreno, S.; Munoz-Páez, A. *J. Phys. Chem. B* **1998**, *102*, 3272–3282.
(12) Finney, J. L.; Soper, A. K. *Chem. Soc. Rev.* **1994**, *23*, 1–10.
(13) Soper, A. K.; Howells, W. S.; Hannon, A. C. *ATLAS Analysis of Time-of-Flight Diffraction Data from Liquid and Amorphous Samples*; Rutherford Appleton Laboratory Report: Oxfordshire, UK, 1989; Vol. RAL-89-046.
(14) Soper, A. K.; Luzar, A. *J. Chem. Phys.* **1992**, *97*, 1320–1331.
(15) Sears, V. F. *Neutron News* **1992**, *3*, 29–37.
(16) Soper, A. K. *Chem. Phys.* **1996**, *202*, 295–306.
(17) Soper, A. K. *Phys. Rev. B* **2005**, *72*, 104204.
(18) Berendsen, H. J. C.; Grigera, J. R.; Straatsma, T. P. *J. Phys. Chem.* **1987**, *91*, 6269–6271.
(19) Krienke, H.; Opalka, D. *J. Phys. Chem. C* **2007**, *111*, 15935–15941.
(20) Soper, A. K. *Chem. Phys.* **2000**, *258*, 121–137.
(21) Tongraar, A.; Tangkawanwanit, P.; Rode, B. M. *J. Phys. Chem. A* **2006**, *110*, 12918–12926.
(22) Bowron, D. T.; Diaz-Moreno, S. *J. Phys. Chem. B* **2007**, *111*, 11393–11399.
(23) Bowron, D. T. *Mater. Sci. Eng., B* **2008**, *149*, 166–170.
(24) Bowron, D. T. *Pure Appl. Chem.* **2008**, *80*, 1211–1227.
(25) Ankudinov, A. L.; Ravel, B.; Rehr, J. J.; Conradson, S. D. *Phys. Rev. B* **1998**, *58*, 7565–7576.
(26) Wilson, K. R.; Tobin, J. G.; Ankudinov, A. L.; Rehr, J. J.; Saykally, R. J. *Phys. Rev. Lett.* **2000**, *85*, 4289–4292.

JP904382N